

# Self-organization process in newborn skin organoid formation inspires strategy to restore hair regeneration of adult cells

Mingxing Lei<sup>a,b,c,d</sup>, Linus J. Schumacher<sup>e,f</sup>, Yung-Chih Lai<sup>d</sup>, Wen-Tau Juan<sup>d,g</sup>, Chao-Yuan Yeh<sup>a</sup>, Ping Wu<sup>a</sup>, Ting-Xin Jiang<sup>a</sup>, Ruth E. Baker<sup>e</sup>, Randall Bruce Widellitz<sup>a</sup>, Li Yang<sup>b,c,1</sup>, and Cheng-Ming Chuong<sup>a,d,1</sup>

<sup>a</sup>Department of Pathology, Keck School of Medicine, University of Southern California, Los Angeles, CA 90033; <sup>b</sup>111 Project Laboratory of Biomechanics and Tissue Repair, College of Bioengineering, Chongqing University, Chongqing 400044, China; <sup>c</sup>Key Laboratory of Biorheological Science and Technology of the Ministry of Education, College of Bioengineering, Chongqing University, Chongqing 400044, China; <sup>d</sup>Integrative Stem Cell Center, China Medical University Hospital, China Medical University, Taichung 40402, Taiwan; <sup>e</sup>Mathematical Institute, University of Oxford, Oxford OX2 6GG, United Kingdom; <sup>f</sup>Department of Life Sciences, Imperial College, London SW7 2AZ, United Kingdom; and <sup>g</sup>Institute of Physics, Academia Sinica, Taipei 11529, Taiwan

Edited by Elaine Fuchs, The Rockefeller University, New York, NY, and approved July 11, 2017 (received for review January 19, 2017)

**Organoids made from dissociated progenitor cells undergo tissue-like organization. This *in vitro* self-organization process is not identical to embryonic organ formation, but it achieves a similar phenotype *in vivo*. This implies genetic codes do not specify morphology directly; instead, complex tissue architectures may be achieved through several intermediate layers of cross talk between genetic information and biophysical processes. Here we use newborn and adult skin organoids for analyses. Dissociated cells from newborn mouse skin form hair primordia-bearing organoids that grow hairs robustly *in vivo* after transplantation to nude mice. Detailed time-lapse imaging of 3D cultures revealed unexpected morphological transitions between six distinct phases: dissociated cells, cell aggregates, polarized cysts, cyst coalescence, planar skin, and hair-bearing skin. Transcriptome profiling reveals the sequential expression of adhesion molecules, growth factors, Wnts, and matrix metalloproteinases (MMPs). Functional perturbations at different times discern their roles in regulating the switch from one phase to another. In contrast, adult cells form small aggregates, but then development stalls *in vitro*. Comparative transcriptome analyses suggest suppressing epidermal differentiation in adult cells is critical. These results inspire a strategy that can restore morphological transitions and rescue the hair-forming ability of adult organoids: (i) continuous PKC inhibition and (ii) timely supply of growth factors (IGF, VEGF), Wnts, and MMPs. This comprehensive study demonstrates that alternating molecular events and physical processes are in action during organoid morphogenesis and that the self-organizing processes can be restored via environmental reprogramming. This tissue-level phase transition could drive self-organization behavior in organoid morphogenies beyond the skin.**

hair neogenesis | stem cells | phase transition | environmental reprogramming | tissue engineering

**R**ecent studies have made substantial progress in 3D organoid cultures. Multiple epithelial organoids have been generated that resemble their counterparts *in vivo*, such as the mammary gland (1, 2), salivary gland (3), stomach, colon, pancreas ducts, and liver bile ducts (4). Using stem cell biology approaches, scientists have also generated the cerebral cortex (5) and optical cup (6). Common features of these organoids are that they are generated by 3D culture of isolated tissue progenitors or pluripotent stem cells and that a proper environmental context is provided to guide cells to differentiate into multiple cell types with proper tissue organization. These cultures start from dissociated cells that have lost external cues; amazingly, they can still reform organized tissues similar to those produced during embryonic development *in vivo*, albeit with different degrees of tissue organization compared with the normal organ morphology.

Organoid cultures have been used as a disease model and can provide organized tissues for regenerative medicine (7). However,

organoid formation also provides a unique opportunity, which is not fully developed, to decipher fundamental principles of the self-organization processes (8). Self-organization is the spontaneous formation of ordered structures from a group of progenitor cells that have no ordered prepattern. This can be viewed as a developmental biology question: how do embryonic cells organize in different ways to generate diverse organs and body forms (9)? It is clear that we do not fully understand how 1D DNA codes generate 3D organized topologies (10). The genetic codes do not encode morphology directly; instead complex tissue architectures are achieved through several intermediate layers of interactions involving physical and genetic mechanisms (11, 12). How such genetic information and physical processes cross talk and intertwine with one another to achieve morphological phenotypes remains to be elucidated. However, this knowledge has significant implications for improving our ability to deliver more complex organoids.

The skin organ is a consummate model for studying self-organization processes because of its accessibility to experimentation, its relatively flat configuration, and the availability of genetic tools in mice (13–15). Previous studies have shown that a

## Significance

**This study opens avenues to improve the ability of adult skin cells to form a fully functional skin, with clinical applications. Our investigation elucidates a relay of molecular events and biophysical processes at the core of the self-organization process during tissue morphogenesis. Molecules key to the multistage morphological transition are identified and can be added or inhibited to restore the stalled process in adult cells. The principles uncovered here are likely to function in other organ systems and will inspire us to view organoid morphogenesis, embryogenesis, and regeneration differently. The application of these findings will enable rescue of robust hair formation in adult skin cells, thus eventually helping patients in the context of regenerative medicine.**

Author contributions: M.L., R.B.W., L.Y., and C.-M.C. designed research; M.L., P.W., and T.-X.J. performed research; C.-Y.Y. contributed new reagents/analytic tools; L.J.S., Y.-C.L., R.E.B., and C.-M.C. analyzed data; and M.L., L.J.S., W.-T.J., R.B.W., and C.-M.C. wrote the paper.

The authors declare no conflict of interest.

This article is a PNAS Direct Submission.

Data deposition: The sequence reported in this paper has been deposited in the National Center for Biotechnology Information Gene Expression Omnibus (GEO) database, <https://www.ncbi.nlm.nih.gov/geo/> (accession no. GSE86955).

<sup>1</sup>To whom correspondence may be addressed. Email: cmchuong@usc.edu or yanglibme@cqu.edu.cn.

This article contains supporting information online at [www.pnas.org/lookup/suppl/doi:10.1073/pnas.1700475114/-DCSupplemental](http://www.pnas.org/lookup/suppl/doi:10.1073/pnas.1700475114/-DCSupplemental).



dermal cell layers forming skin spheroids. The polarized aggregates become cystic at day 3, filled with keratin, here stained by eosin.

Stage 3, coalesced cysts: Epidermal cell bridges link the cysts, which fuse to form epidermal planes, around day 4–5.

Stage 4, planar skin: The small epidermal planes further merge to form a large plane from day 5.5–7. Notably, at about day 5.5–6, the large plane forms a bilaterally symmetric double-layered epidermal structure with each layer covered by dermal layers facing the liquid or air phase, respectively. The large epidermal planes further coalesce and descend to the bottom of the culture insert at the liquid phase, forming stratified layers from day 6–10. The epidermal and dermal planes are clearly distinguished by epidermal and dermal markers, respectively (*SI Appendix, Fig. S1 F and G*).

Stage 5, hair placode induction: At day 10–11, hair placode-like structures are induced (*SI Appendix, Fig. S1H*). Robust hair follicles with normal structures are regenerated when this explant is transplanted onto the back of a nude mouse, and the regenerated hair follicles are derived from donor cells (*Fig. 1D*). Interestingly, when we culture the cells in a submerged condition, the epidermal cells can also self-organize, as do those in the air–liquid culture condition. The epidermal plane is also formed at the culture insert side (*SI Appendix, Fig. S1I*).

The ratio of epidermal to dermal (E:D) cells influences epidermal cell aggregation (*SI Appendix, Fig. S2A*). Compared with aggregate formation using combinations of epidermal and dermal cells (1:9 ratio), very small aggregates form when only epidermal cells are cultured, indicating that the self-organization process is dermal cell-dependent. We assumed that a higher E:D ratio would lead to larger aggregate formation. Unexpectedly, a higher E:D ratio causes smaller aggregates to form, and vice versa. We next sought to isolate pure epidermal and dermal populations using FACS. Mixed cultures of pure populations from FACS-sorted K14–GFP<sup>+</sup> epidermal and Pdgfra–EGFP<sup>+</sup> dermal cells at a ratio of 1:9 produced similar-sized aggregates (*SI Appendix, Fig. S2 B and C*).

**Adult Cells Fail to Self-Organize.** When adult mouse cells are used in a parallel mixed-cell reconstitution assay, epidermal cells form only a few small aggregates, which do not grow, as demonstrated by immunostaining for specific markers (*Fig. 1 E and F and SI Appendix, Fig. S2D*). Lowering the E:D cell ratio to 1:30 produces larger aggregates which undergo terminal differentiation and fail to coalesce at day 4 (*SI Appendix, Fig. S2E*). Transplanting those adult cells at different E:D ratios to the dorsum of nude mice produced very few hairs compared with the robust hair follicle regeneration seen with newborn mouse cells (*Fig. 1D and SI Appendix, Fig. S2E*). These assays demonstrate that cells from newborn mice have a greater capacity for self-organization and tissue regeneration in this assay than cells derived from older (>2-mo-old) mice and that the self-organization capacity of cells is required for prospective tissue regeneration.

To further confirm that dermal cells are required for epidermal cell self-organization, we performed a recombination assay, including newborn epidermal cells plus adult dermal cells (NE+AD) and newborn dermal cells + adult epidermal cells (ND+AE). The result shows that the ND+AE group undergoes a self-organization process more similar to that of the newborn mouse cells (*SI Appendix, Fig. S2F*). The epidermal cells form small aggregates at day 1, which grow larger and form cysts at day 3. Partial cysts undergo coalescence at day 4 and form a double-layered epidermal plane at day 7. However, the epidermal cells from the NE+AD group form very small aggregates at day 1, which cannot further polarize at day 3 or coalesce at day 4, resulting in terminal differentiation at day 7. When transplanted

onto the nude mice, those cells form very few hairs compared with the ND+AE group, which form numerous hairs.

**Live Imaging of Cellular Behaviors During Organoid Formation.** To observe how cells behave in this assay, we set up a time-lapse live-imaging system using fluorescent confocal microscopy to visualize and quantify cell motility (*SI Appendix, Fig. S3A*). Five major stages of cellular behaviors were observed before hair placode induction based on live imaging of K14–GFP mouse (25) cells showing the epidermal basal component (*Movie S1*).

- i) Dissociated cells. Cells are dissociated at the very beginning.
- ii) Aggregation. During random epidermal cell movement from 0 h to 3 h (*Movie S1*), two or more cells will collide. These cellular contacts lead to the formation of aggregates at day 2 that progressively increase in size. Interesting observations were made during epidermal cell aggregation: (a) Modes of aggregate formation: Large aggregates form through the random addition of single cells, by merging two or more small aggregates, or by a combination of these two mechanisms (*Fig. 2A and SI Appendix, Fig. S3B*). (b) Shape of aggregates: Aggregates form as round balls with a coarse surface. (c) Unstable fusion of aggregates: At 7–12 h cells form aggregates (*Fig. 2A*), but a few aggregates are unstable. Live imaging shows cells or small aggregates can join an aggregate and then leave (*Fig. 2A*, purple arrow and *SI Appendix, Fig. S3 C–E*); however, aggregation is far more frequent than dissociation, so overall aggregates form and grow. Small aggregates also can merge to form larger aggregates (*Fig. 2B*). Rarely, large aggregates can disaggregate into smaller components (*Fig. 2C*).

Cell tracking revealed that epidermal cells move in an undirected manner, i.e., with low directional persistence, throughout the experiment (*Fig. 2E*). Furthermore, cell velocities decrease as more cells are in clusters. Thus, we were motivated to describe epidermal cell aggregation, as a first approximation, using the Smoluchowski coagulation equations with a size-dependent aggregation rate (*SI Appendix, Fig. S3F*). Numerical solutions to these equations match aggregate cluster size distributions from the initial stage of the aggregation process (*Fig. 2F*). The only free parameter in this model is the overall aggregation rate constant. In addition to fitting the numerical solution to the data, we collapse the size distributions from different time points onto a single curve (*SI Appendix, Fig. S3G*) by rescaling relative to the average cluster size at each time point, thus confirming the aggregation model in a parameter-free manner. Size distributions from the 48-h time point do not scale as predicted by the theory (*SI Appendix, Fig. S3G*), indicating a change in cluster growth dynamics during the transition to stage 2, when aggregates develop polarity and interact with dermal cells through the formation of a basement membrane.

- iii) Polarization. Cell aggregates stop growing when the outer epidermal cells become crescent-shaped, suggesting the polarization of aggregates and the conversion of cell aggregates into cysts (*Fig. 2 B and C*). At this time, the epidermal cysts are encircled with two or three layers of dermal cells that show dynamic and random movements (*Fig. 2D and Movie S2A*).
- iv) Coalescence. With increasing time, more and more cells undergo apoptosis in the center of the aggregate, forming a cyst, while some outer cells still dynamically circle around the aggregate (*Fig. 2G*). The cystic aggregates start a dynamic merging process at about day 4, which can occur through two means: (a) nearby aggregates can directly merge together (*SI Appendix, Fig. S3H and Movie S2B*) and (b) a group of epidermal cells protrudes from more distant aggregates, leading to the coalescence of cysts (*Fig. 2H*).



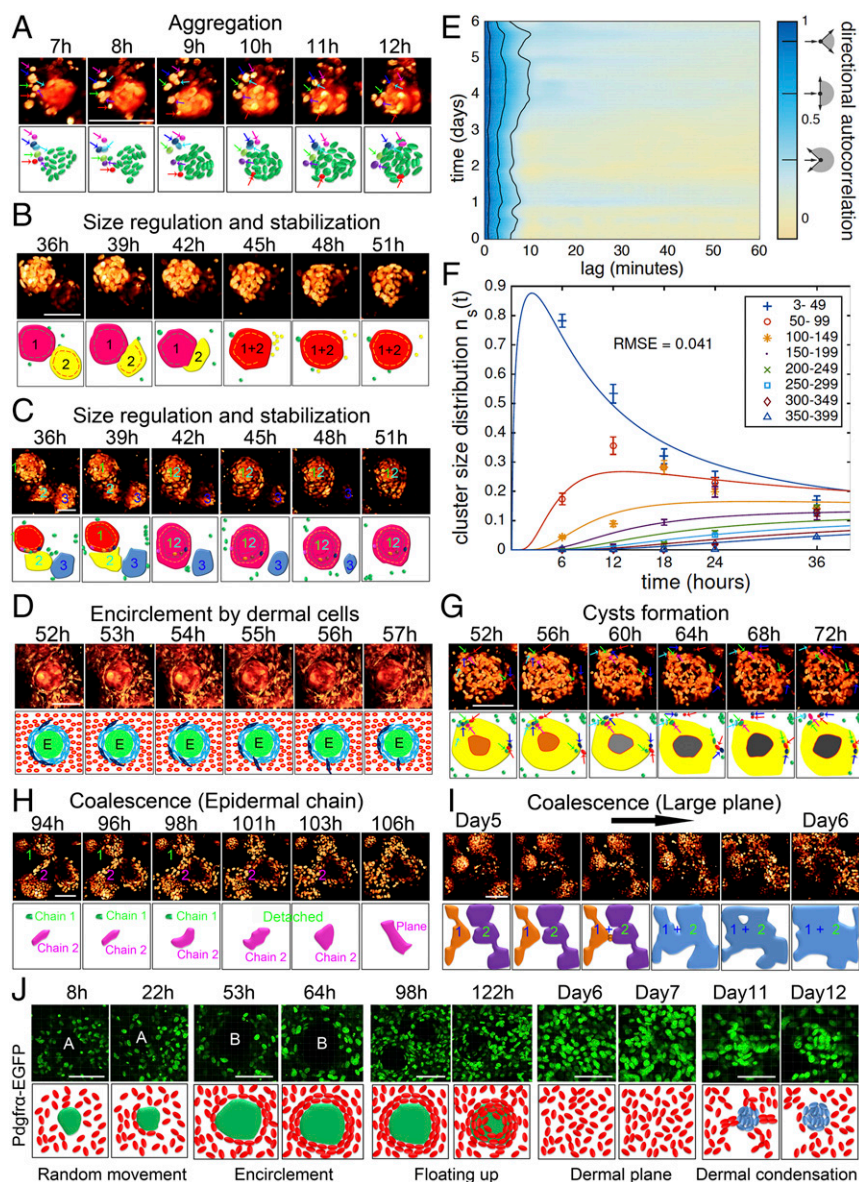


**Fig. 2.** Exemplary analyses of collective cell behavior during self-organization are shown schematically. (See time-lapse live-imaging [Movie S1](#) and [S3](#) for visualization of epidermal and dermal cells using K14-GFP or Pdgfra-EGFP transgenic mouse lines, respectively.) (A) Aggregate formation. Most cells enter the aggregates, but a few enter and then leave the aggregates. (Scale bar, 100  $\mu$ m.) (B) Two aggregates merge together to form a larger aggregate and form concentric layers. (Scale bar, 100  $\mu$ m.) (C) Three aggregates merge. Later, one detaches while the other two form a larger, stabilized aggregate. (D) An epidermal aggregate is surrounded by two or three dermal cell layers, which are dynamic, as shown by FVB-GFP mouse cells. (E) Epidermal cells move with low persistence throughout the experiment, as shown by directional autocorrelation of tracked cells. Black lines show the autocorrelation expected when angles are randomly chosen from the range indicated by the schematics next to the color bar. (F) Numerical fit of the aggregation model to the change in epidermal cell cluster size distribution for the first 36 h. (G) Cyst-like cavity formation in the center of the aggregate. Cells in the center of the aggregate undergo apoptosis, while other cells leave and join the aggregates. (H) Aggregates protrude epidermal cell chains to coalesce together. Not all aggregates merge at the same time. (I) Fused aggregates further coalesce to form a larger epidermal plane. (J) Time-lapse live imaging of Pdgfra-EGFP mouse cells shows dermal cell behaviors. (Scale bars, 100  $\mu$ m.)  $n \geq 50$ .

v) Planar skin formation. The merged cysts continue to coalesce to form an even larger plane, through the protrusion of an epidermal chain or by adjacent fusion of smaller planes (Fig. 2I). Then the lower epidermal plane becomes differentiated at day 7. From day 9 to day 10 the epidermal cells become relatively quiescent again ([Movie S1](#)).

We also examined dermal cell behavior by observing Pdgfra-EGFP mouse cells ([Movie S3](#)), which represent all dermal cell lineages (26). Six major stages were observed comparable to the stages in epidermal cells (Fig. 2J):

- Dissociated cells (0 h).
- Random movement and initial association with epidermal cells: At 8 h, most of the dermal cells remain dissociated and move quickly and randomly. A few cells become associated with the dark region representing the epidermal aggregate.
- Encirclement of dermal cells around the epidermal cyst: A subpopulation of dermal cells forms single to multiple layers of concentric circles surrounding the epidermal cells from day 1 to day 4. This was also visualized by using a FVB-GFP mouse in which all the cells fluoresce ([Movie S24](#)).

- Reorganization: As the epidermal cysts merge, the dermal cells move away from the interaggregate region ([Movies S2B](#) and [S3](#)). The dermal cells then gradually move up above the epidermal cells to the air phase from day 4 to day 10.
- Dermal plane formation: The dermal cells gradually cover all the epidermal cells and form the dermal plane. By using a K14-GFP/Lef1-RFP transgenic mouse, we show that Lef1<sup>+</sup> papillary dermal cells are located adjacent to K14<sup>+</sup> epidermal cells ([Movie S2C](#)). The dermal cells become more quiescent when the dermal plane forms at day 7 and is maintained through day 10.
- Dermal condensation: Some dermal condensates are observed at days 11–12 ([Movies S2C](#) and [S3](#)).

**Transcriptome Profiling During the Self-Organization Process to Form Skin.** To explore the molecular basis of the self-organization process, we performed RNA-sequencing (RNA-seq) in duplicate at seven time points ([SI Appendix, Fig. S4A](#)), showing six groups of genes that were differentially expressed at different stages (Fig. 3A and [SI Appendix, Fig. S4A–C](#) and [Table S1](#)). Those genes were further classified into four major categories based on cellular processes (Fig. 3B).

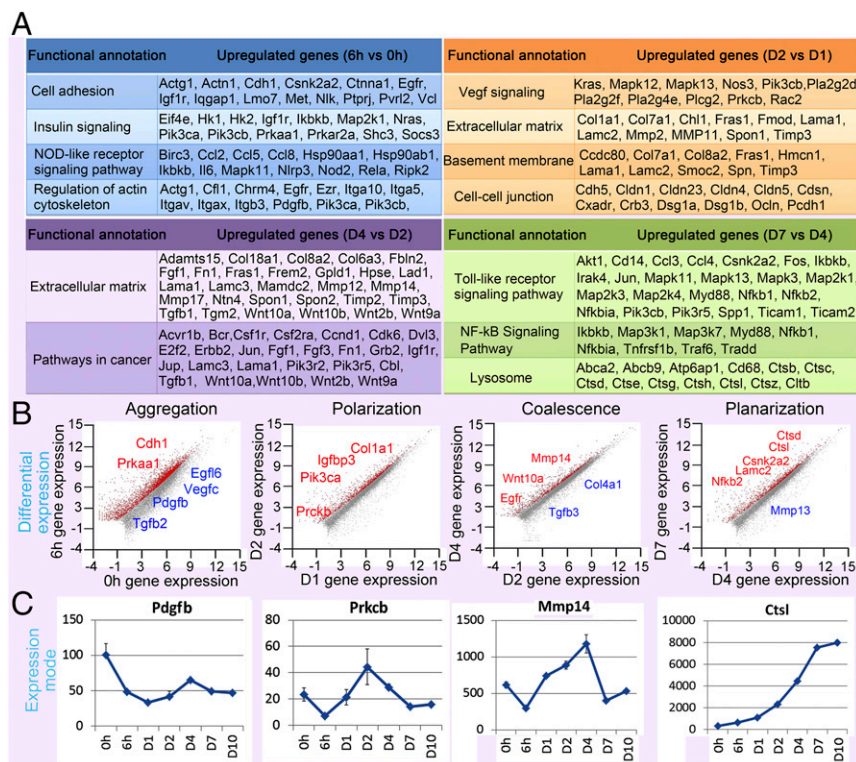


**Fig. 3.** RNA-seq profiling and bioinformatics analysis reveal key molecular changes at different times during the self-organization process. RNA-seq data are from 0 and 6 h and days 1, 2, 4, 7, and 10. (A) Functional annotations show pathways and genes that are increased at different time points. Gene ontology shows that cell adhesion-, insulin signaling-, and NOD-like receptor signaling pathway-related genes are differentially expressed at 6 h. Vegf signaling-, extracellular matrix-, and basement membrane-related genes are differentially expressed at day 2. Another group of ECM genes is differentially expressed at day 4. Toll-like receptor-, Nf-κB signaling pathway-, and lysosome-related genes are differentially expressed at day 7. (B) Gene-expression changes during the key stages. Genes labeled in red are significantly increased, and those labeled in blue are significantly decreased at different stages. (C) Examples of the molecular expression sequence from transcriptome profiling. *Pdgfb* is significantly decreased at 6 h. *Prkcb*, *Mmp14*, and *Ctsl* are significantly increased at day 2, day 4, and day 7, respectively.

- i) **Aggregation:** Known principles of organ self-assembly are based on the sorting of cells with similar adhesive properties, where differential cell fate decisions are due to distinct spatial distributions (7, 8). Indeed, in our system, RNA-seq data show adhesion molecules such as *Cdh1* were highly expressed at the initial stage at 6 h (Fig. 3B and *SI Appendix, Fig. S4D*). Besides, gene ontology shows that genes involved in the insulin-signaling pathway (e.g., *Prkaa1*, *Pik3ca*) and NOD-like receptor signaling pathways (e.g., *Pdgfb*) are also increased at 6 h (Fig. 3 and *SI Appendix, Fig. S4D*). At day 1, many collagen genes are increased (e.g., *Col1a1*, *Col4a1*), and another group of cell adhesion and focal adhesion genes (e.g., *Pik3r1*) is up-regulated (*SI Appendix, Fig. S4 C and D*).
- ii) **Polarization:** At 48 h, the polarized aggregate stage, several genes involved in the IGF (e.g., *Igfbp3*) and Vegf (e.g., *Vegfc*, *Prkcb*) signaling pathways are up-regulated. Additional extracellular matrix (ECM) genes (e.g., *Col4a1*) are increased at day 2 (Fig. 3B and C and *SI Appendix, Fig. S4D*). Genes involved in basement membrane formation and cell-cell junctions are also enhanced.
- iii) **Coalescence:** At day 4, some extracellular matrix molecules, including Wnt family members (e.g., *Wnt10a*), are increased (Fig. 3 and *SI Appendix, Fig. S4D*). Wnts are reported to induce MMP expression (27, 28). Indeed, we observed that a group of MMP genes (e.g., *Mmp13*, *Mmp14*) is expressed at this time point (Fig. 3 and *SI Appendix, Fig. S4D*). In contrast, collagen genes, including *Col1a1* and *Col4a1* and those involved in TGF signaling (e.g., *Tgfb3*), are down-regulated (Fig. 3B and C and *SI Appendix, Fig. S4D*). The cellular behavior of epidermal cell coalescence resembles cancer cell invasion. Interestingly, gene ontology shows pathways involved in cancer are significantly increased at this stage (Fig. 3A).
- iv) **Planar skin formation:** When planar skin was formed from day 6 to day 10, we found that many genes (e.g., *Nfkb2*) involved in Toll-like receptor signaling are up-regulated, and genes related to NF-κB signaling and lysosome-mediated ap-

optosis (e.g., the *Ctsl* family) are increased (Fig. 3 and *SI Appendix, Fig. S4 C and D*). At day 10, another group of epidermal differentiation complex (EDC) genes carrying precursors for cornified envelope, such as the *Spr* gene family members, is increased (*SI Appendix, Fig. S4 C and D*).

- v) **Hair primordia:** Hair follicle development-related genes such as multiple Wnt genes (e.g., *Ctnnb1*, *Wnt3a*, and *Wnt5a*) are increased, which might initiate periodic patterning (*SI Appendix, Fig. S4 C and D*). Hair follicle morphogenesis was largely investigated in previous studies (29); thus, we focused on the earlier stages in the present study.

**Spatiotemporal Genes Expression During the Self-Organization Process.** To investigate the spatiotemporal expression of genes identified by RNA-seq, we performed immunostaining and in situ hybridization. We chose the specific genes and pathways based on three principles. (i) The functional annotation of the selected pathway should have significance ( $P < 0.05$ ). (ii) The genes in those pathways selected for immunostaining or in situ hybridization should be at a detectable level. For this, we checked the gene expression by looking at their RPKM (reads per kilobases per million reads) value (usually larger than 25 for gene-expression studies). (iii) The phenotypes observed in the morphological transition processes were also matched with functional annotations to target the potential genes or pathways in these top enriched pathways.

We observed that adhesion molecules, including β-catenin, neural cell adhesion molecule (NCAM), P-cadherin (*Cdh3*), and E-cadherin (*Cdh1*), are strongly expressed in the epidermal cells, particularly at the border of the cyst (Fig. 4A and *SI Appendix, Fig. S5 A and B*). We also selected one sample gene representing each highly enriched signaling pathway for testing by in situ hybridization. The results show that *Igfbp3*, *Vegfa*, and *Tgfb1* are expressed in the dermis surrounding the epidermal aggregates (*SI Appendix, Fig. S5C*). A basement membrane forms at the outer part of the cyst, shown by collagen type I and type IV, and



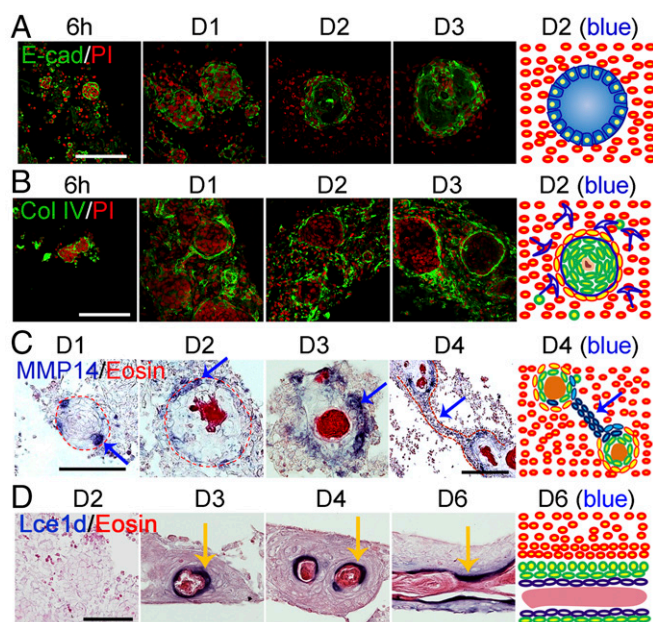


**Fig. 4.** Spatiotemporal molecular expression pattern during the self-organization process. (A) Immunostaining shows E-cadherin is highly expressed at 6 h and is decreased in the center of the aggregate at day 2. (B) Immunostaining shows dynamic changes in collagen IV expression. (C) In situ hybridization shows *Mmp14* is expressed at both the basal layer of the aggregate at day 1 and in dermal cells adjacent to the aggregate (day 2–3) or in dermal cells aligned between aggregates (day 4). (D) In situ hybridization shows that the epidermal differentiation gene *Lce1d* is expressed at the suprabasal layers of aggregates and planar skin. (Scale bars, 100  $\mu$ m.)  $n = 9$ .

Lamc2 expression (Fig. 4B and *SI Appendix*, Fig. S5D). Many cells in the center of the cyst undergo apoptosis and stop proliferating after day 2 (*SI Appendix*, Fig. S5D).

At day 4, during epidermal aggregate coalescence, the chain of cells that protrudes from the aggregates expresses E-cadherin, P-cadherin,  $\beta$ -catenin, Dsc3, and Dsg3 (*SI Appendix*, Fig. S5E), indicating its epidermal identity. MMPs may play a role in breaking the basement membrane to release the epidermal cells from the aggregate. We tested *Mmp14* and *Mmp13* expression, which was highly up-regulated based on our RNA-seq analysis. *Mmp14* is observed both in the basal layer of the aggregate and in the dermal cells surrounding the aggregate at day 3.5. Also, *Mmp14* expression was occasionally observed in the dermal chain (Fig. 4C). *Mmp13* is preferentially expressed at the liquid phase of the aggregates from day 3.5 (*SI Appendix*, Fig. S5F).

The inner part of the cyst fuses together after the cyst coalesces. In situ hybridization shows genes involved in epidermal differentiation are expressed in this same region, which becomes the suprabasal layer of the planar skin (Fig. 4D and *SI Appendix*, Fig. S5G).

In summary, the spatiotemporal expression of molecules in both epidermal and dermal cells may trigger epidermal and dermal interactions in different phases. For example, the dermal microenvironment secretes ECM, including collagens that facilitate basement membrane formation at day 2, and then is broken by the MMPs at day 4, which may lead to the dynamic cellular behaviors observed between stage 1 and stage 4 during the self-organizing planar skin-forming process (*SI Appendix*, Fig. S5H). Our findings suggest that different classes of molecules are required to transition between different stages of skin organoid morphogenesis. It should be noted these are early events that precede periodic formation of hair primordia.

## Molecular Perturbation of the Skin Organoid Formation Process.

**From dissociated cells to cellular aggregates.** To determine the possible involvement of the differentially expressed genes in regulating the switch of morphological phases, we carried out functional perturbation by applying small molecule inhibitors or recombinant proteins highlighted by RNA transcriptome analyses in the cultures at different time points.

Small aggregates formed from epidermal cells alone without dermal cells (*SI Appendix*, Fig. S2A), but they failed to grow larger, indicating that dermal signals are required for further epidermal cell aggregation. *Pdgfb*, which is secreted by dermal fibroblasts, started to be increased at 6 h. The aggregate size was significantly increased at day 1 and day 2 when inhibitors of *Pdgfb* or *Pdgf* receptors were applied at 0 h (Fig. 5A and B and *SI Appendix*, Fig. S6A and B). *Pik3cg*, involved in the IGF pathway, was reported to be an important modulator of extracellular signals, including those elicited by E-cadherin-mediated cell–cell adhesion (30). Inhibiting PI3K function with Ly294002 resulted in larger aggregate formation (*SI Appendix*, Fig. S6A and B). Conversely, the aggregate size was significantly decreased when IGF (e.g., *Igf2*, and *Igf1r*) and VEGF (e.g., *Vegf2* and *Vegfrs*) family members were inhibited (Fig. 5A and B, *SI Appendix*, Fig. S6A and B, and *Movie S4* for IGF inhibition).

**From cell aggregates to coupled epidermal–dermal cysts.** The apical–basal polarity of aggregates formed at day 2. To test whether collagens are involved in this process, we added recombinant collagen I or IV proteins to the cells. These proteins homed to the dermal cell region and displayed longer fibers at day 1 (*SI Appendix*, Fig. S6C). The results reveal collagen I and IV have at least two functions during epidermal aggregation. Live imaging showed the formation of a long epidermal cell strand with some epidermal cells migrating along the strand when recombinant collagen I protein was added to the cells at day 1 (*SI Appendix*, Fig. S6D and *Movie S5A*), indicating that collagen fibers may facilitate epidermal cell movement and bridge aggregates which then merge together. Later, cells treated with recombinant collagen I or IV protein formed more concentric aggregate layers at day 2 and day 3 (Fig. 5C, *SI Appendix*, Fig. S6E, and *Movie S5B*), suggesting that those collagens promote aggregate assembly. P-cadherin immunostaining showed that aggregate apical–basal polarity formation was accelerated after collagen types I and IV protein treatment (Fig. 5C and D and *SI Appendix*, Fig. S6E), with very smooth border formation at day 1 compared with the coarse border found in control samples. Interestingly, aggregates with smooth borders formed at day 1 when inhibitors of TGF $\beta$ -RI, PKR, and class III tyrosine kinase were added at 0 h (*SI Appendix*, Fig. S6F and *Movie S6* for TGF $\beta$ -RI). Atypical PKC was reported to be involved in epidermis polarity formation (31). After PKC activity is inhibited with Bisindolylmaleimide, P-cadherin immunostaining reveals that aggregate size is unaffected but polarity is lost (Fig. 5C and D).

**Coalescence of cysts.** During the coalescence stage (around day 4), a group of epidermal cells protrudes from the aggregates. This process can be accelerated by inhibiting EGF signals or activating Wnt signaling (Fig. 5E and F and *SI Appendix*, Fig. S7A and B). When inhibitors or agonists targeting these pathways were added to the culture at day 1, 70% of aggregates coalesced by day 3, compared with ~15% in controls (Fig. 5E and F and *SI Appendix*, Fig. S7A and B).

We next pursued how the polarized aggregates coalesce. The basement membrane of the aggregate needs to break to release epidermal cells. We speculated that MMPs play a role in this process. Indeed, when the MMP inhibitor Prinomastat was added to the cultures, live imaging of K14-GFP epidermal cells showed blocked aggregate coalescence at day 3.5 (Fig. 5E and F and *Movie S7A–C*). This also was evidenced by imaging cellular behaviors of *Pdgfra*-EGFP-labeled dermal cells, which show

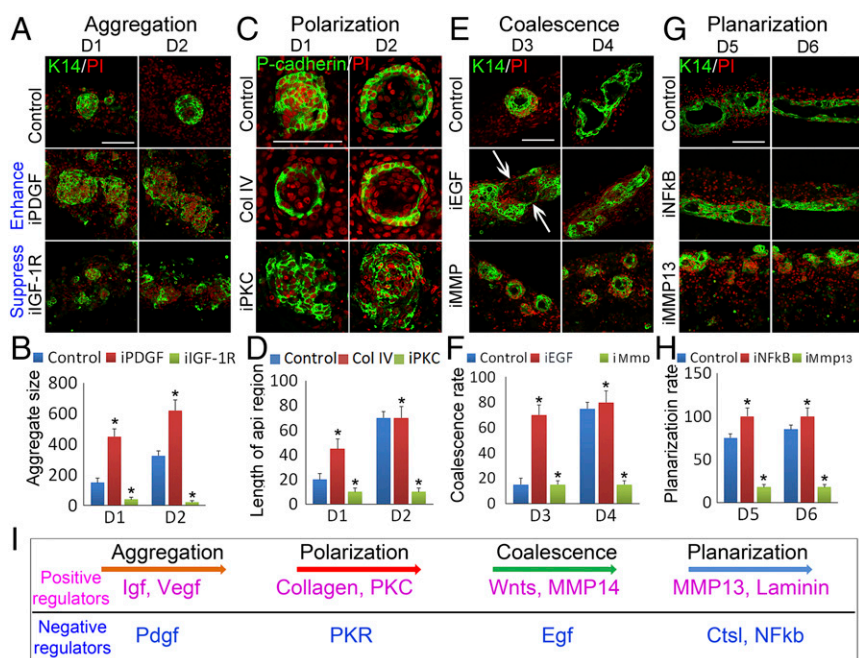


**Fig. 5.** Functional perturbations at different times elucidate molecules that can accelerate or suppress different phase-transition stages. (A and B) Aggregates are enlarged or decreased in size when treated with PDGFR (iPDG) or IGF-1R (iIGF-1R) inhibitors, respectively. Cells are immunostained with K14. (C and D) P-cadherin immunostaining shows the apical-basal polarity formation is accelerated or disrupted by treatment with collagen type IV recombinant protein or PKC inhibitor (iPKC), respectively. D1 represents cells cultured for 1 day, similarly hereinafter. (E and F) K14 immunostaining and live-imaging show that coalescence of the aggregates is accelerated or blocked by treatment with EGF inhibitor (EGF) or MMP (iMMP) inhibitor (Prinomastat), respectively. (G and H) Planarization of the aggregates is accelerated or blocked by treatment with NFκB inhibitor (iNFκB) or MMP13 inhibitor (iMMP13), respectively. (Scale bars, 100 μm.) \* $P < 0.05$ ,  $n = 9$ . (I) Schematic of molecular modules involved in the transitions between different morphological stages. Positive (in purple) and negative (in blue) regulators work in balance to move the process forward.

dermal cell movement and blocking of epidermal aggregate coalescence (SI Appendix, Fig. S7C and Movie S7 D and E). **Lamella formation.** The cysts descend to the bottom of the culture insert at day 6. We wondered whether the differential expression pattern of *Mmp13* (SI Appendix, Fig. S5F) might be involved in this process. When the selective potent MMP13 inhibitor Way 170523 was added, the aggregates showed less coalescence and failed to descend to the liquid phase (Fig. 5 G and H). From RNA-seq data, we observed increased *Nfkb2* and *Ctsl* expression at the coalescence stage. K14 immunostaining reveals that specific inhibitor-mediated protein inactivation facilitates cyst coalescence and promotes the sinking of cysts (Fig. 5 G and H and SI Appendix, Fig. S7D). In addition to influencing smooth border formation of the aggregates (Movie S8), laminin, which is normally highly expressed at day 4, is required to promote further coalescence of the small epidermal plane to form a large epidermal plane. Inhibition of laminin blocked further coalescence (SI Appendix, Fig. S7D and Movie S8). Together, the positive and negative molecular modules at different time points direct the progression of self-organization during skin organoid formation (Fig. 5I).

#### Dermal Cells Used for Periodic Patterning Are from Papillary Dermis.

In addition to epidermal cell patterning, we examined which dermal cell population enhanced planar skin formation in culture. *Lrig1* and *Dlk1* are expressed in the upper and lower dermis, respectively, during skin development. Those different populations have different hair follicle-regenerative abilities during reconstitution (32). In the present study, RNA-seq data showed that *Dlk1* expression was quickly lost at day 1, and *Lrig1* was decreased but was maintained at a certain level during culture, indicating that the dermal cells of the reconstituted skin originated from the upper dermis (SI Appendix, Fig. S7E). Using a K14-GFP/Lef1-RFP mouse in the reconstitution assay, we observed that Lef1-RFP<sup>+</sup> cells that belong to the papillary dermis were located adjacent to the epidermal plane (SI Appendix, Fig. S7F, Upper and Movie S2C). This is also indicated by Lef1 immunostaining, which shows that three or four layers of Lef1<sup>+</sup> cells are located beside the epidermal plane (SI Appendix, Fig. S7F, Lower). These dermal cells can form dermal condensate-like structures that are alkaline phosphatase-positive (SI Appendix, Fig. S7G). The dermal con-

densate was also observed by culturing skin cells from a Sox2-EGFP transgenic mouse at day 11 (SI Appendix, Fig. S7G). Transplanting these cultures into nude mice results in the formation of hair follicles with irregular spacing between each hair follicle, compared with the evenly spaced buds between hair follicles that are physiologically developed during embryogenesis in mouse (SI Appendix, Fig. S7H). This suggests the reconstituted skin is competent to form new placodes, but competence in different parts of the explants may not be achieved at the same time, giving rise to the irregular pattern observed here. More studies will be needed to investigate this phenomenon further.

#### Rescuing the Hair Regeneration Ability of Adult Mouse Skin Cells by Restoring the Self-Organization Process.

We further tested whether the principles governing morphological transitions in newborn mouse cells could be applied to restore the self-organizing abilities of adult mouse cells (>2 mo old) to form hair-bearing skin. We performed RNA-seq using adult-cell-derived organoid cultures and compared the results with those using newborn cells at corresponding time points (SI Appendix, Fig. S8 A–D). Both newborn and adult cells can form small aggregates, but adult cell aggregates stall before the aggregates grow larger (Fig. 1 E–G). As such, we selected genes that are up-regulated in both newborn cells and adult cells at 6 h that foster cell aggregation and genes up-regulated only in newborn cells but not in adult cells at day 1 and day 2 that may be responsible for later phase-transition-like events (Fig. 6A and SI Appendix, Fig. S8 C and D).

The gene ontology results show that genes involved in the *Igf* and *Vegf* signaling pathways are highly enriched in both newborn and adult cells at 6 h but are up-regulated in newborn cells compared with adult cells at day 1 and day 2 (SI Appendix, Fig. S8E). Some Wnt genes such as *Rspo2*, *Wnt3a*, and *Wnt10b* are also expressed at a higher level in newborn cells (Fig. 6A). The biggest difference we observed is that adult cells quickly differentiate in culture. Compared with the newborn culture, in which epidermal differentiation genes become enriched at later stages (D7), many EDC genes start to be enriched from 6 h or day 1 in adult cultures (Fig. 6B and SI Appendix, Fig. S8F), which could be one of the main reasons that cells lose their competence to regenerate hairs and terminally differentiate.



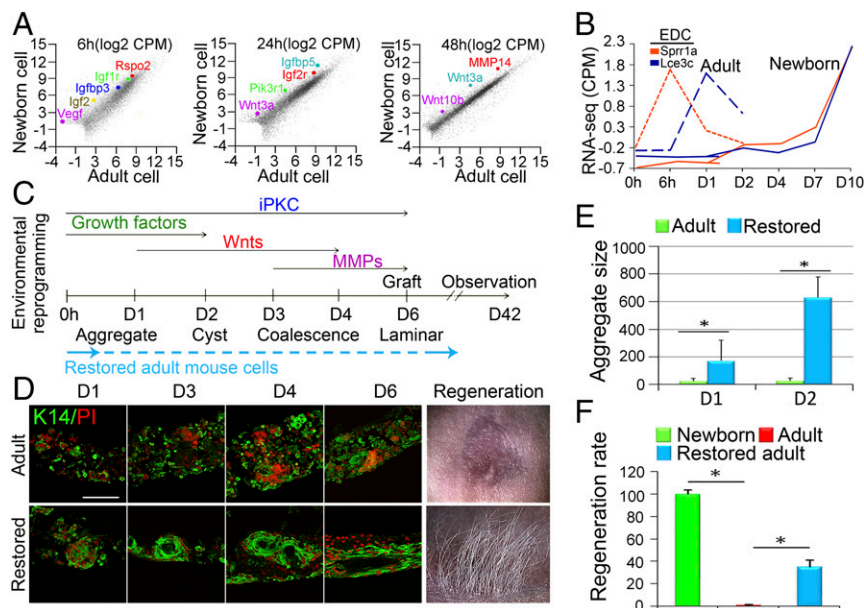


**Fig. 6.** Environmental reprogramming of adult cells to generate hair-bearing skin. (A) RNA-seq profiling shows major differences between newborn and adult mouse cells. *Igf1*, *Vegf*, and *Wnt*-related genes are highlighted at different time points. (B) EDC genes (e.g., *Sprr1a* and *Lce3c*) are not highly expressed until day 7 in newborn cultures but begin to increase at 6 h in adult cultures. (C) Based on these findings, we designed the optimal environmental reprogramming protocol to deliver key molecules at different stages. See *SI Appendix, Fig. S8* for comprehensive data. PKC inhibitors (iPKC) are added throughout to suppress epidermal differentiation. Growth factors IGF2, IGFBP3, and VEGF2 recombinant proteins are added first from days 0–2. Wnt3a or Wnt10b is then added daily from days 1–4. MMP13 and MMP14 are added at days 3–6. Then the cultures are transplanted onto nude mice. (D) Adults' cells now progress through morphological transition to form cysts and coalesce. (Scale bar, 100  $\mu$ m.) (E) Adults' cells now form larger aggregates in vitro. (F) Significantly more hairs are regenerated when treated adult cell cultures are transplanted onto the backs of nude mice. \* $P < 0.05$ ,  $n = 9$ .

Based on transcriptome analyses and functional studies, we have found that altering the expression of just one molecule at a time does not produce impressive advances in restoring hair formation. Here, guided by our concept learned from newborn skin cultures, we are able to design a systemic pathway to restore the organoid formation process. We set up a stepwise method to reinduce the self-organization process per our RNA-seq analyses (Fig. 6C). We first added multiple growth factors, including IGF and VEGF, at the initial stage. We then added Wnt3a or Wnt10b recombinant proteins at day 1, due to their dual function in newborn cells, including enlarging aggregate size and accelerating aggregate coalescence, and their reduced expression in adult cells. Also, we added MMPs from day 3 to trigger the coalescence of aggregates. Importantly, to prevent epidermal cell differentiation, we added PKC inhibitors throughout the whole cultivation period.

The results show that the addition of IGF2, IGFBP3, or VEGF2 recombinant proteins led to an enlarged aggregate size (Fig. 6D and E and *SI Appendix, Fig. S8 G–I*). Strikingly, a single addition of IGF2, IGFBP3, or VEGF2 recombinant proteins is sufficient to induce aggregates to enlarge significantly in size at day 1 and day 2, but then they terminally differentiate at day 3 (*SI Appendix, Fig. S8G*), indicating those factors can enhance cell adhesion but cannot maintain planar skin-forming properties. The addition of Wnt3a or Wnt10b recombinant proteins at day 1 further increases aggregate size at day 2 and induces epidermal cell chain protrusions at day 3. In fact, a single addition of Wnt3a or Wnt10b at time 0 is also sufficient to enlarge aggregate size at day 2, although with a probability of less dense hair regeneration upon transplantation (*SI Appendix, Fig. S8 J and K*). Coalescence of aggregates occurred when MMP14 recombinant protein was added subsequently. These coalesced aggregates can descend directly to the liquid phase and form symmetric epidermal layers, indicating that signals involved in aggregate descent are induced. These “restored” adult organoids were then transplanted to the dorsum of nude mice, where regeneration of hair follicles increased from 0 to around 40% of the levels seen with newborn cell organoid cultures (Fig. 6D and F and *SI Appendix, Fig. S8H*,  $n = 9$ ). K14-GFP shows the regenerated hair follicles are derived from donor cells (*SI Appendix, Fig. S8L*).

## Discussion

**The Self-Organizing Process of Planar Skin Formation from Dissociated Cells Is Counterintuitive.** We have developed a 3D in vitro organoid model in which dissociated newborn mouse skin cells are cultured at high density. This gives us the unique opportunity to visualize the process leading from individual cells to skin with time-lapse movies. Within a 10-d period, we observed that the dissociated cells progress through a series of morphological phase transitions to achieve a planar layer of presumptive skin with hair primordia (Fig. 7). Grafting of this explant to nude mice with a full-thickness skin wound leads to well-formed reconstituted skin with robust hair growth. These hair follicles have normal architecture and can

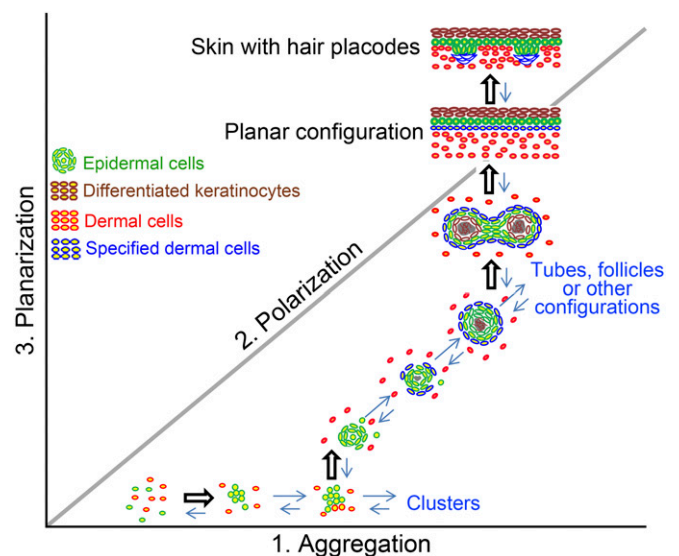


**Fig. 7.** Hypothetical morphospace showing the many possible multicellular configurations that take place during morphogenesis of organoid skin cultures. In this space, each axis represents a major change of cell properties and distinct configuration. The self-organization process from dissociated cells to hairy skin can be viewed as a trajectory. Switching of molecular activity is required to move cell collectives from one phase to the next (represented by open arrows).



undergo cyclic regeneration, fulfilling the definition of tissue-engineered hair follicles (19, 24).

However, close inspection of this process revealed two surprises. First, in skin development, presumptive skin covers the body surface; then periodically arranged dermal condensation and epidermal placode start to emerge around embryonic day 14. In vitro, it is remarkable, because the dissociated cells, having lost all external cues in developing embryos, can reroute and traverse a different morphogenetic path to acquire the same phenotype they have in vivo. This is not what one would expect if morphogenesis were to occur based on a simple molecular blueprint. Instead, it indicates that more fundamental self-organization principles are followed by the dissociated cells to achieve their final morphology.

Second, planar skin has a simple configuration consisting of an epidermis and a dermis, with a basement membrane in between. Thus, one may intuitively consider that dissociated epidermal and dermal cells, mixed in suspension, could simply sort themselves out and form sandwich-like cellular layers. Instead, the cells in our assay take a tortuous route from dissociated cells  $\rightarrow$  aggregate  $\rightarrow$  polarized cysts  $\rightarrow$  coalescing cysts  $\rightarrow$  planar hair-bearing skin. We postulate that direct formation of the final, layered skin may well violate the physical constraints imposed by the nature of the active material that the mixture of cells constitutes. Instead, the morphological phase-transition-like events we describe here may represent the most efficient, feasible way for cells to self-organize along a path of least resistance. Intuitively, the straight line is the shortest distance between two points. However, in the morphospace of multicellular configurations (Fig. 7), a straight path may not be the shortest path: It may be easier for cells to take a winding route through a landscape of possible tissue architectures. What, then, are the guiding principles that determine this route?

**Tissue-Level Morphological Phase Transitions.** Here we look at the phenomenon of multicellular self-organization from the biophysicists' perspective, borrowing the concepts of phase transitions at the tissue level. The term "phase transition" is most commonly used to describe the transformation of matter from one phase/state to another as a function of changes in internal variables or the environment. Phase transitions have recently been shown to mediate cytoplasmic organization at the sub-cellular level. The assembly and disassembly of nucleoli and other nuclear bodies cycle between liquid-phase droplets and solid-phase condensations and can be modulated by rRNA transcription (33). Phase transition of the microtubule-associated zinc finger protein plays an essential role in the assembly of the spindle apparatus and its associated components (34).

It is compelling to extend this biophysical concept to multicellular self-organization. We consider cells in our assay as particles with certain surface properties, performing a random walk (approximately, see Fig. 2E) in a crowded 3D environment. There are two major particle categories, epidermal (E) and dermal (D), so the major interparticle interactions are E-E, D-D, and E-D. Initially epidermal cells form aggregates. When these aggregates reach a certain size, apical-basal polarity develops, leading to the formation of a cyst-like structure. This apical-basal polarity means the inner core and the outer shell of the cyst exhibit different affinities to the environment. Outside the cyst, the interaction of basement membrane with dermal fibroblasts and the presence of MMPs destabilize the cyst structure. The merging of cysts, the fusion of smaller lamellar planes, and thus the eventual large-scale planar configuration may simply be a straightforward consequence of interactions between cell aggregates whose physical properties are changing over time. The biophysical analogy we draw here, although the size scale and dynamics are different from those in soft-matter systems,

may shed light on how the system self-organizes into different multicellular configurations.

### Molecular and Physical Events of Organoid Formation from Newborn Skin Inspire a Strategy to Restore Hair Formation in Adult Mice.

To profile the molecular events associated with the observed morphological transitions, we analyzed the skin cells' transcriptome. We found that there are four peaks of molecular expression, each corresponding to a tissue phase transition: growth factors for the aggregate formation stage (days 0–2); ECM including collagens for apical-basal polarity and cyst formation (days 1–4); Wnts and MMPs for coalescence of the aggregates (days 3–6); and NF $\kappa$ B and laminin for tissue remodeling in the planar formation stage (days 6–10) (Figs. 3 and 4). Functional perturbation with inhibitors of the key molecules at each phase-transition stage can suppress or accelerate the phase-transition process (Fig. 5).

The components of these organoid cultures are difficult to dissect. Instead of getting into spatial dissection, we decided to do time-point analyses of the whole culture first. This analysis will provide us with the first level of information about which molecular pathways are important for the morphological transition between stages.

Cells from adult mouse skin are quiescent and normally fail to form hairs. Within the logic of our biophysical analogy, we reasoned that we should be able to restore the phenotype by supplying the necessary molecules to the adult cells to reestablish phase-transition-like self-organization behaviors. We examined the cellular and molecular properties of adult cells to find ways to restore their morphogenetic ability. By mapping the cell configuration back to the morphospace of Fig. 7, we can appreciate that adult cell cultures are stuck in the aggregation phase ( $x$  axis). By RNA-seq, we found that epidermal differentiation genes appear at an early stage. To restore the ability of adult cells to form hair-bearing skin, we designed a protocol based on the knowledge derived from newborn cell cultures. First, we added inhibitors to PKC to keep cells in undifferentiated states longer. Then we sequentially added three categories of molecules: (i) IGF2/Vegf, (ii) Wnt3a and Wnt10b, and (iii) MMP14 recombinant proteins at days 0, 1, and 3, respectively, to facilitate progression through the morphogenetic stages. In this way, keratinocyte differentiation is reduced. Thus, under the induction of these sequentially added proteins, the morphological transitions are reestablished, and adult cells become competent to reconstitute skin that, upon transplantation, forms hairs robustly.

We identified multiple positive and negative regulatory modules directing the progression of morphological transitions during skin organoid formation (Fig. 5I). Instead of focusing on a single molecule, we think the successive phase-transition-like events are the key to successful self-organization (Fig. 6D). More generally, dissociated cells can self-assemble to form many possible multicellular configurations (cell aggregates, cysts, tubes, sheets, and other configurations) in a hypothetical morphospace (Fig. 7). Between each phase, activators and inhibitors work as a feedback control to stop the earlier phase and initiate the next phase. Thus, simply getting bigger cell aggregates is not useful if they do not progress into cyst stage.

The morphospace in Fig. 7 can also be useful to appreciate the diverse morphogenetic phenotypes by different epithelial organoids. For example, reconstituted primary mammary myoepithelial cells and luminal cells can form glandular cystic aggregates when placed on Matrigel substrates (2, 35). However, when FGF2 is provided, the cysts undergo branching morphogenesis (36) and do not coalesce toward a planar configuration. In the present study, the end point is a planar skin with hairs. These results suggest there are molecular specificities among different cell types that steer the transitions through morphospace to different multicellular configurations.

In summary, we propose that the combined use of molecular signals and biophysical processes may be a basic principle used by nature to drive morphological transitions from one phase to the next. It is the progression of these phase switches, not the specific molecules, that is the key to the success of self-organization. By analyzing more examples of organoid morphogenesis in this context, we stand to learn more about how different physical principles are combined with intrinsic cellular properties to achieve self-organization, thus enhancing our ability to apply these principles to advance tissue engineering.

## Materials and Methods

**In Vitro Assay.** As shown in Fig. 1A, cells were prepared according to our previously described method (19). Usually, the E:D ratio in a piece of back skin from a newborn mouse is about 1:9 when we dissociate the back skin into single cells. For the preparation of adult cells, the skins ( $n \geq 3$ ) from 2-mo-old mice, in which hair follicles are at refractory telogen phase, were peeled off before the hair fibers were plucked through waxing. Then the s.c. fat was removed from the skins by scissors, and the skins were floated on a 0.25% trypsin solution at 4 °C for overnight digestion. The epidermis was scrapped off the dermis by a scalpel. Then epidermis and dermis were dissociated into single cells as in the preparation of newborn cells. The dissociated epidermal cell and dermal cells were mixed at a ratio of 1:9 and were dropped onto a Transwell culture insert (Fisher Scientific) that was put in a six-well culture plate. The lower part of the culture insert was filled with 1.5 mL DMEM/F12 (1:1) (Gibco) culture medium containing 10% FBS (Gibco). The cells were cultured in a humidified atmosphere containing 5% CO<sub>2</sub> at 37 °C, with the culture medium being changed every other day. All animal procedures were performed upon approval of the University of Southern California (USC) Institutional Animal Care and Use Committee.

**Live Imaging and Analysis.** As shown in *SI Appendix*, Fig. S3A, cells were cultured on a Transwell insert placed in a glass culture plate. The plate was

covered by a latex membrane to avoid evaporation of the culture medium. The system was kept at 37 °C by placing the plate on a heating platform and by heating the lens, which was immersed in the culture medium. A LSM5 meta confocal microscope was used to film the cellular behaviors. The resulting 4D (3D space plus time) cellular images were then tracked using commercially available Imaris software (Bitplane) at the Broad California Institute for Regenerative Medicine (CIRM) Center at the University of Southern California.

Complete methods and any associated references are available in *SI Appendix*.

**ACKNOWLEDGMENTS.** We thank Drs. Qing Liu and Justin Ichida at the CIRM Center of the USC for supporting the small molecule inhibitors; the USC Epigenome Core Facility for conducting Illumina transcriptome sequencing; the USC Norris Medical Library Bioinformatics Service for assisting with sequencing data analysis; and Prof. Philip Maini of the University of Oxford, Dr. Philip Murray of the University of Dundee, members of the devBio discussion group at the Wolfson Centre for Mathematical Biology, Dr. Christoph Weber of the Max Planck Institute for the Physics of Complex Systems, Drs. Tian Yang and Xiaohua Lian of the Third Military Medical University, Dr. Chin-Lin Guo of Academia Sinica, and Dr. Maksim V. Plikus of the University of California, Irvine for helpful discussions. C.-M.C., R.B.W., T.-X.J., and P.W. are supported by NIH Grants AR42177 and AR60306. M.L. is supported by Project 2016M590866 funded by the China Postdoctoral Science Foundation, Fundamental Research Funds for the Central Universities Grant 106112015CDJRC231206, Special Funding for Postdoctoral Research Projects in Chongqing Grant Xm2015093, and Fellowship 2011605042 from the China Scholarship Council. L.Y. is supported by Innovation and Attracting Talents Program for College and University (111 Project) Grant B06023 and National Nature Science Foundation of China Grants 11532004 and 31270990. W.-T.J. is supported by the Academia Sinica Research Project on Nanoscience and Technology and the Ministry of Science and Technology of Taiwan. L.J.S. was funded by UK Engineering and Physical Sciences Research Council Grant EP/F500394/1 through a studentship at the Life Sciences Interface Programme of the University of Oxford's Doctoral Training Centre.

- Lo AT, Mori H, Mott J, Bissell MJ (2012) Constructing three-dimensional models to study mammary gland branching morphogenesis and functional differentiation. *J Mammary Gland Biol Neoplasia* 17:103–110.
- Cerchiari AE, et al. (2015) A strategy for tissue self-organization that is robust to cellular heterogeneity and plasticity. *Proc Natl Acad Sci USA* 112:2287–2292.
- Joraku A, Sullivan CA, Yoo J, Atala A (2007) In-vitro reconstitution of three-dimensional human salivary gland tissue structures. *Differentiation* 75:318–324.
- Sato T, Clevers H (2015) SnapShot: growing organoids from stem cells. *Cell* 161:1700–1700.e1.
- Eiraku M, et al. (2008) Self-organized formation of polarized cortical tissues from ESCs and its active manipulation by extrinsic signals. *Cell Stem Cell* 3:519–532.
- Eiraku M, et al. (2011) Self-organizing optic-cup morphogenesis in three-dimensional culture. *Nature* 472:51–56.
- Lancaster MA, Knoblich JA (2014) Organogenesis in a dish: Modeling development and disease using organoid technologies. *Science* 345:1247125.
- Sasai Y (2013) Cytosystems dynamics in self-organization of tissue architecture. *Nature* 493:318–326.
- Chuong CM, Richardson MK (2009) Pattern formation today. *Int J Dev Biol* 53:653–658.
- Edelman GM (1989) Topobiology. *Sci Am* 260:76–82, 84–86, 88.
- Newman SA, Bhat R (2008) Dynamical patterning modules: Physico-genetic determinants of morphological development and evolution. *Phys Biol* 5:015008.
- Bhat R, Bissell MJ (2014) Of plasticity and specificity: Dialectics of the microenvironment and macroenvironment and the organ phenotype. *Wiley Interdiscip Rev Dev Biol* 3:147–163.
- Fuchs E (2009) Finding one's niche in the skin. *Cell Stem Cell* 4:499–502.
- Rompolas P, Greco V (2014) Stem cell dynamics in the hair follicle niche. *Semin Cell Dev Biol* 25:26:34–42.
- Jiang TX, et al. (2004) Integument pattern formation involves genetic and epigenetic controls: Feather arrays simulated by digital hormone models. *Int J Dev Biol* 48:117–135.
- Lichti U, et al. (1993) In vivo regulation of murine hair growth: Insights from grafting defined cell populations onto nude mice. *J Invest Dermatol* 101(1, Suppl):1245–1295.
- Zheng Y, et al. (2005) Organogenesis from dissociated cells: Generation of mature cycling hair follicles from skin-derived cells. *J Invest Dermatol* 124:867–876.
- Toyoshima KE, et al. (2012) Fully functional hair follicle regeneration through the rearrangement of stem cells and their niches. *Nat Commun* 3:784.
- Lee LF, Jiang TX, Garner W, Chuong CM (2011) A simplified procedure to reconstitute hair-producing skin. *Tissue Eng Part C Methods* 17:391–400.
- Lei M, Chuong CM (2016) STEM CELLS. Aging, alopecia, and stem cells. *Science* 351:559–560.
- Weber EL, Chuong CM (2013) Environmental reprogramming and molecular profiling in reconstitution of human hair follicles. *Proc Natl Acad Sci USA* 110:19658–19659.
- Higgins CA, Chen JC, Cerise JE, Jahoda CA, Christiano AM (2013) Microenvironmental reprogramming by three-dimensional culture enables dermal papilla cells to induce de novo human hair-follicle growth. *Proc Natl Acad Sci USA* 110:19679–19688.
- Thangapazham RL, et al. (2014) Dissociated human dermal papilla cells induce hair follicle neogenesis in grafted dermal-epidermal composites. *J Invest Dermatol* 134:538–540.
- Chuong CM, Cotsarelis G, Stenn K (2007) Defining hair follicles in the age of stem cell bioengineering. *J Invest Dermatol* 127:2098–2100.
- Tumbar T, et al. (2004) Defining the epithelial stem cell niche in skin. *Science* 303:359–363.
- Collins CA, Kretschmar K, Watt FM (2011) Reprogramming adult dermis to a neonatal state through epidermal activation of  $\beta$ -catenin. *Development* 138:5189–5199.
- Wu B, Crampton SP, Hughes CC (2007) Wnt signaling induces matrix metalloproteinase expression and regulates T cell transmigration. *Immunity* 26:227–239.
- Pukrop T, et al. (2006) Wnt 5a signaling is critical for macrophage-induced invasion of breast cancer cell lines. *Proc Natl Acad Sci USA* 103:5454–5459.
- Lei M, Inaba M, Chuong CM (2016) Vertebrate embryo: Development of the skin and its appendages. *eLS*, 10.1002/9780470015902.a0026601.
- Pastor JC, et al. (2016) Proliferative vitreoretinopathy: A new concept of disease pathogenesis and practical consequences. *Prog Retin Eye Res* 51:125–155.
- Williams SE, Beronja S, Pasolunghi HA, Fuchs E (2011) Asymmetric cell divisions promote Notch-dependent epidermal differentiation. *Nature* 470:353–358.
- Driskell RR, et al. (2013) Distinct fibroblast lineages determine dermal architecture in skin development and repair. *Nature* 504:277–281.
- Berry J, Weber SC, Vaidya N, Haataja M, Brangwynne CP (2015) RNA transcription modulates phase transition-driven nuclear body assembly. *Proc Natl Acad Sci USA* 112:E5237–E5245.
- Jiang H, et al. (2015) Phase transition of spindle-associated protein regulate spindle apparatus assembly. *Cell* 163:108–122.
- Chanson L, et al. (2011) Self-organization is a dynamic and lineage-intrinsic property of mammary epithelial cells. *Proc Natl Acad Sci USA* 108:3264–3269.
- Ewald AJ, Brenot A, Duong M, Chan BS, Werb Z (2008) Collective epithelial migration and cell rearrangements drive mammary branching morphogenesis. *Dev Cell* 14:570–581.